JOURNAL OF MATERIALS SCIENCE 13 (1978) 2147–2156

Crystallization of grain boundary phases in hot-pressed silicon nitride materials

Part 2 *Mechanical properties of materials*

J. E. WESTON*, P. L. PRATT
Department of Metallurgy and Materials Science, Imperial College of Science and Technology, London, UK

The mechanical properties of hot-pressed silicon nitrides containing crystalline magnesium silicate phases were investigated at room temperature and at elevated temperatures. Scanning electron microscopy of fracture surfaces was used to identify the fracture-initiating flaws at room temperature and the modes of fracture at higher temperatures. The mechanical properties of these materials at elevated temperatures were interpreted in terms of a subcritical crack growth mechanism involving grain boundary sliding, which implied the presence of residual glass phases at the grain boundaries.

1. Introduction

Commercial hot-pressed silicon nitrides, which are prepared using magnesium oxide as a densification aid, are believed to contain a magnesium silicate glass as a grain boundary phase [1–4]. This glass phase causes grain boundary sliding to occur in the material under an applied stress at elevated temperatures, and thus the mechanical properties deteriorate at these temperatures [5–8].

Part 1 of this paper [9] described a method for the preparation of hot-pressed silicon nitride and silicon nitride–alumina materials in which crystallization of the magnesium silicate phases was induced by the use of multicomponent oxide mixtures as the densification aid and an *in situ* heat treatment after hot-pressing. In this part of the paper the mechanical properties of two of these materials, at room temperature and at elevated temperatures, are investigated in order to determine the effects of the crystallization of their grain boundary phases.

2. Experimental

2.1. Materials examined

Table I shows the compositions and typical impurity analyses of the two materials examined. These materials were hot-pressed at 1600° C and 22.5 $MN m^{-2}$ for 60 min in graphite dies coated with boron nitride, with an *in situ* heat treatment at 1100° C for 60 min after hot-pressing [9]. The crystalline phases present in the hot-pressed products, identified by X-ray powder analysis, are shown in Table II.

2.2. Measurement of fracture stress

Specimens for three-point bend testing were cut from hot-pressed pellets 38 mm in diameter and approximately 12 mm thick. Each specimen was cut so that its long axis was perpendicular to, and the direction of crack propagation during fracture was parallel to, the hot-pressing axis. The upper and lower faces of each specimen (i.e. the compression and tension faces during bending) were diamond-ground parallel to the long axis. For room temperature testing the specimen dimensions were 3.25 ± 0.25 mm in width, 3.00 ± 0.25 mm in depth and approximately 30 mm in length; for the elevated temperature tests the dimensions were 3.00 ± 0.20 mm, 3.00 ± 0.20 mm and approximately 25 mm respectively. The sharp long edges of the specimen were rounded off on 600 grade silicon carbide abrasive discs to minimize fracture from edge chips during testing.

At room temperature the specimens were tested in air in three-point bending using a standard Instron testing machine. The three-point fixture

*Present address: Department of Metallurgy and Materials Science, University of Cambridge, Pembroke Street, Cambridge, UK.

© *1978 Chapman and Hall Ltd. Printed in Great Britain.*

TABLE I(a) Summary of material impurities

Composition code letter	Si_3N_4 powder grade	Typical impurity content (p.p.m.)					
		Al	Ca	Fe	Mg	K	Na
B	"Controlled phase"	6000	3000	9000	Impurity level unknown		
J	"High purity"	1200	400	650	80	34	11

TABLE I(b) Summary of material compositions

Composition code letter	Si_3N_4 including surface SiO_2 (wt %)	SiO_2 (wt %)	Al_2O_3 (wt %)	CaO (wt %)	MgO (wt %)	TiO_2 (wt %)
B	91.96	2.29	2.76	0.47	1.38	1.14
J	93.61	1.02	2.81	0	1.40	1.16

TABLE II Crystalline phases detected by X-ray analysis

Composition	Crystalline phase detected
B	β-silicon nitride (Si_3N_4), *major*
	Forsterite (Mg_2SiO_4), *minor*
	Silicon oxynitride (Si_2ON_2), *minor*
	Silicon (Si), *trace*
J	β-silicon nitride (Si_3N_4), *major*
	Silicon oxynitride (Si_2ON_2), *medium*
	Enstatite ($MgSiO_3$), *minor*

fitted into a reversing jig bolted to the movable cross-head of the Instron frame. The load was transferred to the specimen via tungsten carbide rollers approximately 3 mm in diameter, which fitted into cylindrical grooves in the fixture. The upper roller was attached to a ram that was free to pivot about an axis parallel to the long axis of the specimen, ensuring a uniform contact of the rollers across the specimen width. The load was applied to the specimen via the upper roller assembly which was driven by the Instron cross-head and the load transmitted to the lower rollers via the specimen was measured using a 500 kg load-cell. Tests were conducted at a cross-head speed of 0.5 mm min^{-1} and with a span of 27.5 mm. The failure stress of each specimen was calculated using:

$$\sigma_f = \frac{3}{2}\frac{WL}{xy^2} \quad (1)$$

where

σ_f = fracture stress ($N m^{-2}$)
W = load at fracture (N)
L = span (m)
$x(y)$ = specimen width (depth) (m).

The apparatus for elevated temperature testing is shown in Fig. 1. The bend test jig, made from reaction-bonded silicon nitride, consisted of upper and lower rams which contained slots into which were fitted knife-edges. The lower knife-edges were located by alumina pegs fitted into the lower ram. This ensured that a specimen placed against the steps on these knife-edges would be perpendicular to the long axes of the knife-edges and directly below the centre of the upper knife-edge. The silicon nitride rams were fitted via steel pins onto water-cooled stainless steel rods so as to allow the rams to pivot to ensure a uniform contact of the knife-edges across the specimen width. The stainless steel rods were fitted to a standard Instron testing frame. The upper rod was attached to a 500 kg compression load-cell and the lower rod rested on a hemispherical ball-bearing in a socket bolted to the cross-head. An induction furnace was placed around the test jig so that the specimen was at the centre of the furnace during

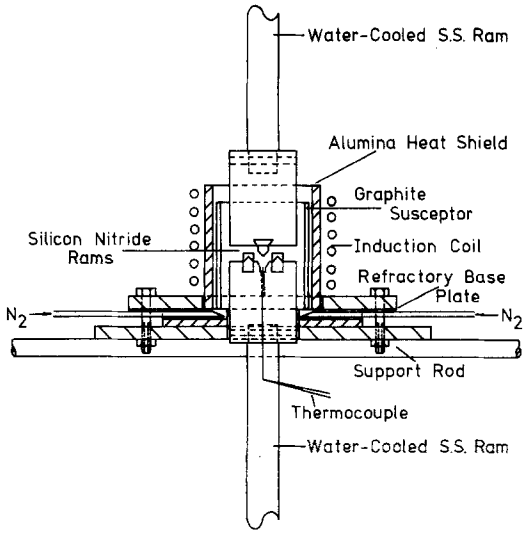

Figure 1 High temperature three-point bend test apparatus.

testing (Fig. 1). Oxygen-free nitrogen was passed between the silicon nitride rams and the graphite susceptor to protect these components from excessive oxidation. The specimen temperature was measured using a Pt/Pt–13% Rh thermocouple with its junction just below the midpoint of the specimen position. The temperature was controlled manually by varying the power output of the r.f. generator and it was found to be possible to hold and reproduce temperatures within ±6° C.

The induction furnace could be raised to allow a specimen to be placed in the bend test jig. The furnace was then lowered and the specimen heated to the testing temperature within approximately 30 min and held at this temperature for 10 min before testing. After the test the apparatus was allowed to cool to about 400° C before the furnace was raised, to protect the fracture faces of the specimen from excessive oxidation.

The load was applied to the specimen via the lower knife-edges (22.15 mm span) which were driven by the Instron cross-head and the load transferred to the upper knife-edge was measured by the load cell. Specimens were tested between room temperature and 1375° C and at cross-head speeds of 0.05, 0.5 and 5.0 mm min^{-1}. The failure stress of each specimen was calculated using Equation 1.

2.3. Measurement of Young's modulus

The plots of load applied against cross-head movement, obtained during three-point bend testing at room temperature and at elevated temperatures, were used to calculate a value of Young's modulus for each specimen. The deflection of the specimen at fracture was found by extrapolation of the straight line portion of the plot back to zero load and the modulus calculated using:

$$E = \frac{WL^3}{4vxy^3} \quad (2)$$

where:

E = Young's modulus ($N\,m^{-2}$)
v = deflection at fracture (m).

The measured deflection had to be corrected for the compliance of the Instron testing frame and bend test jig in each case. This was achieved by finding the deflection at fracture for ten specimens of a well characterized sintered alumina (E = 240 $GN\,m^{-2}$ [10]) with the same dimensions as the sample specimens for each apparatus. As the Young's modulus of the alumina was known only at room temperature it was not possible to calibrate the elevated temperature apparatus above room temperature. However, only the reaction-bonded silicon nitride test jig was located within the furnace so that it was assumed that the compliance of this apparatus was not greatly changed at elevated temperatures.

2.4. Scanning electron fractography

Selected fracture surfaces of specimens tested at room temperature and at elevated temperatures were examined using a standard Cambridge Stereoscan 600 scanning electron microscope in the reflected electron mode. Specimens were gold-coated before examination.

3. Results

3.1. Room temperature fracture

The results of room temperature bend tests on specimens from typical pellets of compositions B and J are shown in Table III. For both compositions, the material was fully brittle and fracture occurred by the extension of existing flaws in the material.

The fracture faces of both materials exhibited clearly defined fracture mirrors surrounded by hackle markings, which enabled the positions of the fracture initiating flaws to be identified. In all the specimens examined, fracture was initiated at

TABLE III Room temperature bend test results

Composition	Density ($Mg\,m^{-3}$)	Mean fracture strength ($MN\,m^{-2}$)	Standard deviation ($MN\,m^{-2}$)	Mean Young's modulus ($GN\,m^{-2}$)	Standard deviation ($GN\,m^{-2}$)	Number of specimens
B (Pellet B3)	3.11	665	55	309	35	11
J (Pellet J2)	3.15	694	52	324	40	11

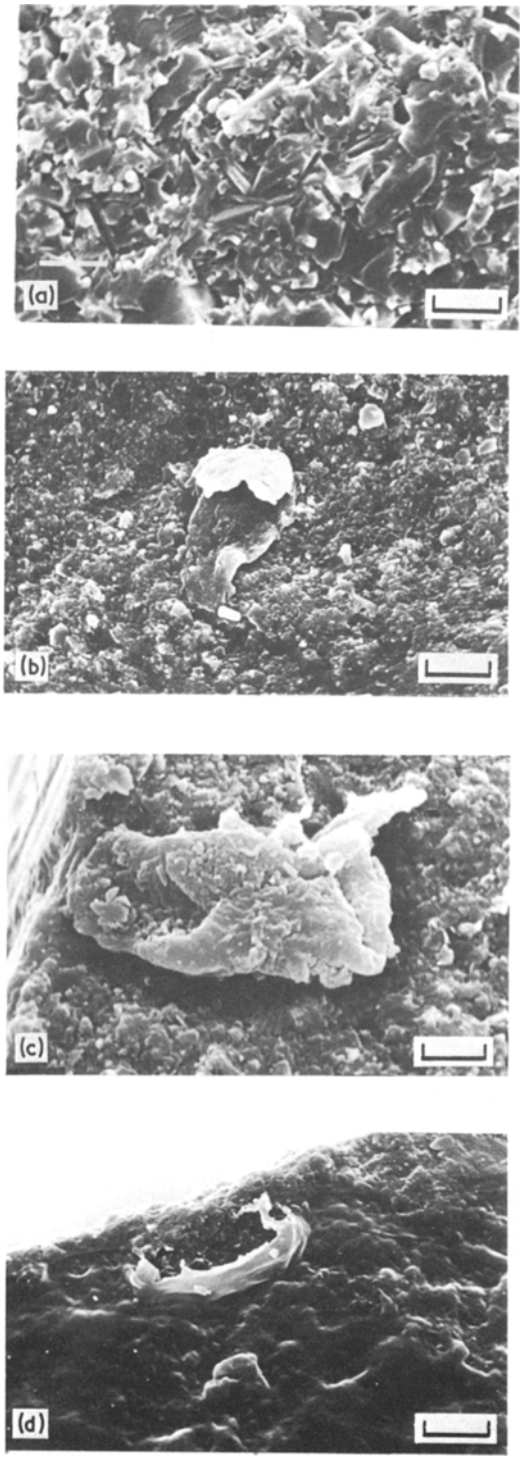

Figure 2 Details of room temperature fracture: (a) Fracture face, composition J, bar = 2 μm; (b) inclusion on fracture face, composition B, bar = 10 μm; (c) fracture-initiating flaw, composition B, bar = 4 μm; (d) fracture-initiating flaw, composition J, bar = 10 μm.

the tensile surface, or within 100 μm of this surface, i.e. in no case was failure initiated at an internal flaw.

Fig. 2a shows details of the fracture face of a specimen of composition J. The fracture mode was mixed, with intergranular fracture predominating, and the microstructure consisted of grains of widely varying grain size (submicron to about 4 μm at the largest dimension) with many of the grains having a high aspect ratio. A very similar type of fracture surface was obtained for specimens of composition B. Inclusions were occasionally present on the fracture faces of both types of material, Fig. 2b. The size of these inclusions varied from about 5 to 40 μm at the largest dimension and they were irregular in shape.

Typical fracture initiating flaws (located at the centres of fracture mirrors) for compositions B and J are shown in Figs. 2c and d. The flaw in Fig. 2c is an inclusion which appears to be separated from the matrix by a circumferential crack, suggesting that this inclusion must have had a higher thermal expansion coefficient that the matrix [11]. Fig. 2d shows a flaw consisting of a surface pore which seems to contain an inclusion of glass or crystallized glass and which is surrounded by a region of abnormally smooth and featureless appearance.

3.2. Elevated temperature fracture

The results of the tests at elevated temperatures are summarized in Figs. 3, 4 and 5. The expermental points are the average of three (occasionally two) results in each case. Fig. 3 shows the bend strengths found using a constant deflection rate (0.5 mm min^{-1}) at a series of temperatures while Fig. 4 gives the results of tests carried out at a series of deflection rates (0.05, 0.5 and 5.0 mm min^{-1}) for two temperatures (1000 and 1200° C). For the latter series of tests the initial outer-fibre stressing rate was determined for each specimen using the formula:

$$\dot{\sigma} = \frac{3}{2}\frac{L}{xy^2}\dot{W}$$

where:

$\dot{\sigma}$ = initial stressing rate (N m^{-2} sec^{-1})
$\dot{W}$ = initial loading rate (N sec^{-1}).

The initial loading rate was found from the initial slope of the load–deflection plot obtained from the recorder of the testing machine. Typical

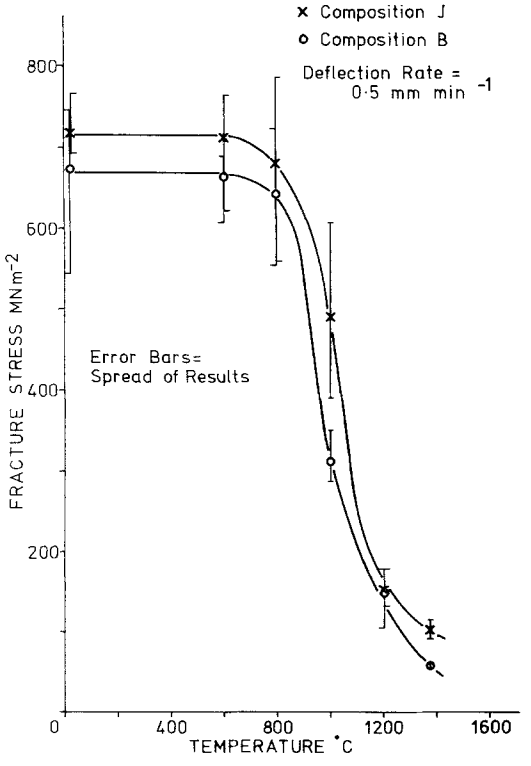

Figure 3 Effect of temperature on the three-point fracture stress.

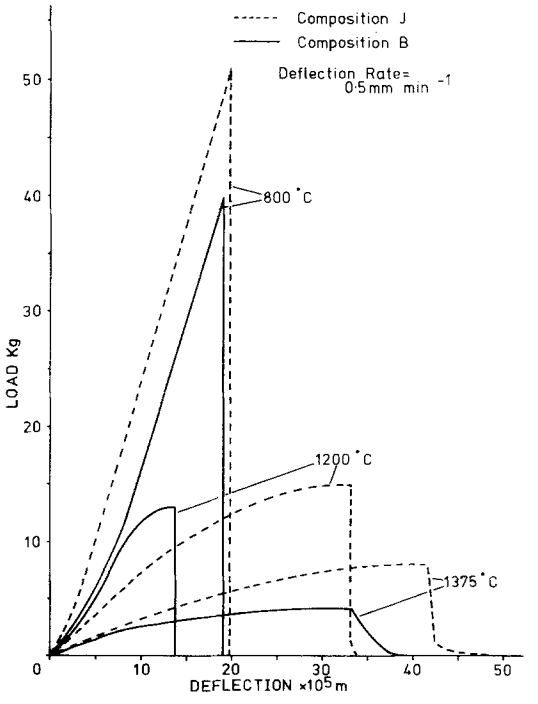

Figure 5 Load versus deflection curves in three-point bending.

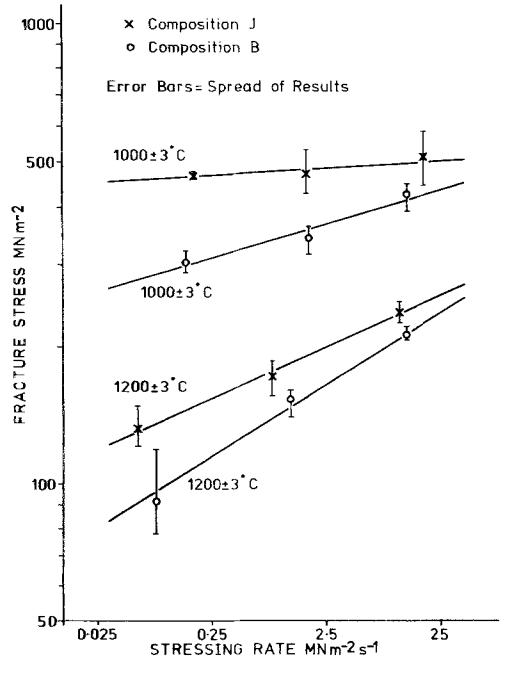

Figure 4 Effect of the initial stressing rate on the three-point fracture stress, 1000 and 1200° C.

load–deflection curves for both compositions at 800, 1200 and 1375° C (0.5 mm min^{-1}) are shown in Fig. 5. These curves were not corrected for the deflection of the testing machine or loading rig during loading.

Owing to the lower strengths of the specimens tested at 1000° C and above, there were few fracture markings on their fracture surfaces and only the specimens of composition J at 1000° C (which had a relatively high strength) produced discernible fracture mirrors. Fig. 6a is a micrograph of the fracture face of a specimen of composition J fractured at 1000° C. Fracture was intergranular and the grain morphology was similar to that of the specimen fractured at room temperature. Similar fracture surfaces were found for specimens of composition B tested at 1000° C. Specimens of both compositions tested at 1200° C produced fracture faces with two distinct regions, Fig. 6b, i.e. a lighter, rougher region showing extensive secondary cracking and a smoother, darker region with little or no secondary cracking. The detailed microstructure of the fracture face was similar in both regions, and for both types of material, and was slightly less sharply defined, Fig. 6c, than for fracture at 1000° C. The depth of the "rough"

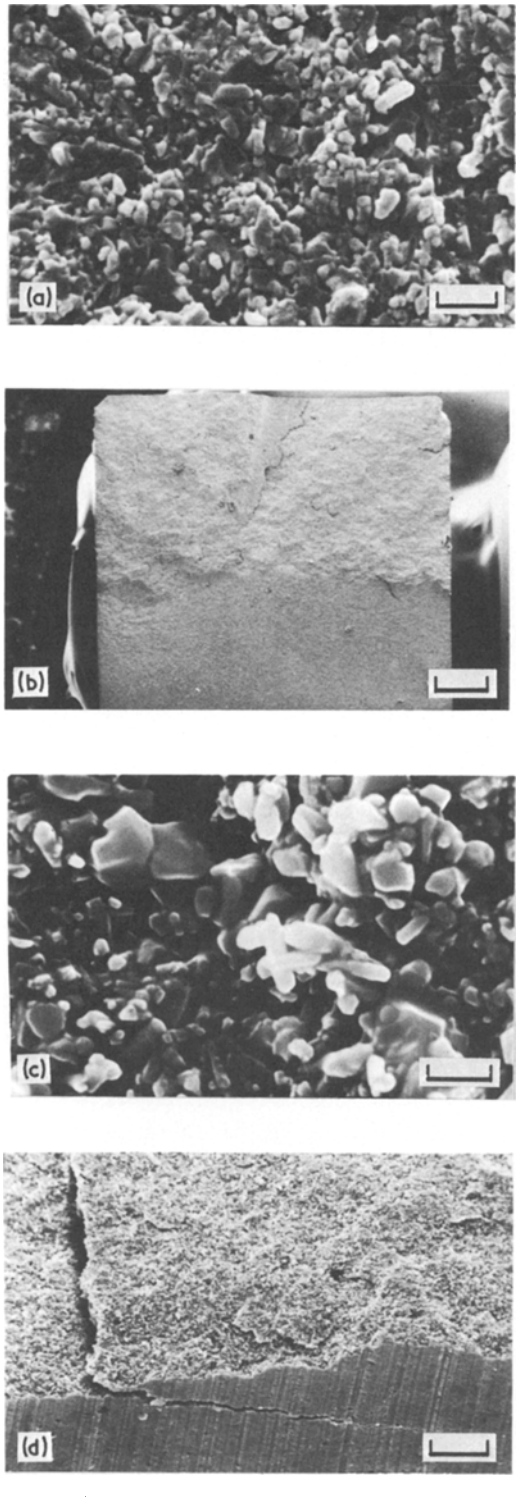

Figure 6 Details of elevated temperature fracture: (a) Fracture face, 1000° C, composition J, bar = 2 μm; (b) fracture face, 1200° C, composition J, bar = 400 μm; (c) fracture face, 1200° C, composition B, bar = 2 μm; (d) secondary cracking, 1375° C, composition J, bar = 40 μm.

region in each specimen tested at 1200° C was measured using an optical microscope fitted with a calibrated graticule, Table IV; the depth of the "rough" region increased as the deflection rate during loading decreased.

Testing at 1375° C produced specimens showing only the "rough" type of fracture surface with very extensive secondary cracking, Fig. 6d. The size of the secondary cracks was generally greater for the specimens of composition B than for those of composition J. For both materials the detailed structure of the fracture faces appeared to be less sharply defined than for specimens fractured at lower temperatures and occasionally the shape of the individual grains was obscured by an amorphous or glassy layer. However, the inclusions that were found on some of the fracture faces of both materials did not appear to have softened or melted after testing at 1375° C. A comparison of Figs. 6a and c shows the difference in grain size between the materials of composition J and composition B and indicates that there was greater grain growth during the hot-pressing of composition B.

3.3. Young's modulus

The values of Young's modulus obtained from the room temperature bend tests were 309 GN m^{-2} for composition B and 324 GN m^{-2} for composition J, Table III.

For the tests at elevated temperatures, it was only possible to make measurements of Young's modulus for each composition up to 1000° C, Fig. 7, as above this temperature the load–deflection curves for both materials were non-linear, Fig. 5.

4. Discussion

4.1. Fracture at room temperature

The fracture strengths of specimens of both compositions (B and J), 665 and 694 MN m^{-2} respectively, are lower than the room temperature three-point bend strengths of the best commercial hot-pressed silicon nitrides, which are typically 800 to 1000 MN m^{-2} [12]. Nevertheless these results are similar to the strength of hot-pressed silicon nitride–magnesia at a similar stage in its development, i.e. 560 to 700 MN m^{-2} [13]. The relatively low strengths of compositions B and J appear to be due to the presence of inclusions which act as fracture-initiating flaws, Fig. 2c. It is likely that these inclusions are forsterite (composition B) and enstatite (composition J), produced by the crystal-

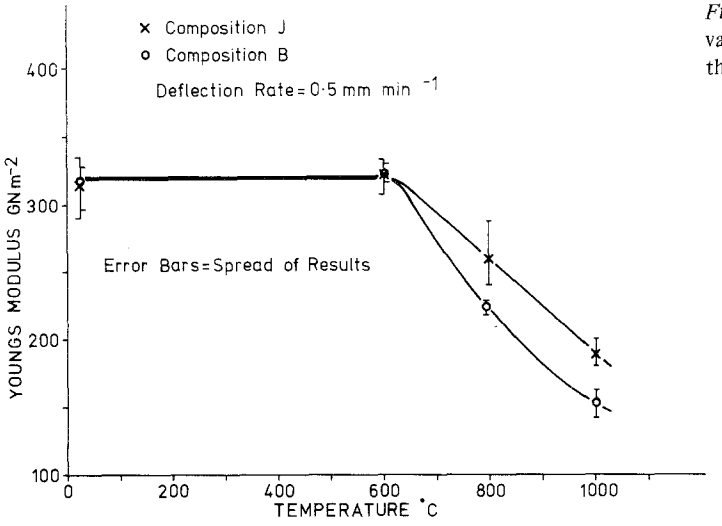

Figure 7 Effect of temperature on the value of Young's modulus measured in three-point bending.

silica on the silicon nitride particles [9]. Thus a reduction in the total amount of liquid phase present during hot-pressing, that is a reduction in the total additive plus surface silica content of the silicon nitride, may prevent the formation of inclusions in this type of material.

Inclusions of either forsterite (α = 9.4 $\times 10^{-6\,\circ} C^{-1}$) or enstatite ($\alpha = 7.8 \times 10^{-6\,\circ} C^{-1}$) in a matrix of β-silicon nitride ($\alpha = 3.2 \times 10^{-6\,\circ} C^{-1}$) would tend to become separated from the matrix by circumferential cracking during cooling from the hot-pressing or heat-treatment temperature [11]. Such an inclusion could then act as a stress intensifier in a manner equivalent to a sharp penny-shaped crack similar in size to the inclusion diameter, and so could initiate fracture. This type of behaviour appears to be indicated in Fig. 2c. The flaw shown in Fig. 2d appears to be a region where

TABLE IV Depth of "rough" region on fracture face of specimens tested at 1200° C

Composition	Deflection rate (mm min^{-1})	Temperature (° C)	Depth of "rough" fracture region (mm)
B	5.0	1201 ± 1	(a) 1.05
			(b) 0.85
			(c) 0.92
	0.5	1202 ± 4	(a) 1.52
			(b) 1.32
			(c) 1.18
			(d) 1.21
			(e) No distinct regions
			(f) 1.30
	0.05	1200 ± 2	(a) Whole fracture face
			(b) Whole fracture face
			(c) 2.89
J	5.0	1200 ± 3	(a) 0.78
			(b) 0.91
			(c) 0.93
	0.5	1200 ± 3	(a) 1.48
			(b) 1.54
			(c) 1.25
			(d) 1.53
			(e) 1.54
			(f) 1.48
	0.05	1201 ± 2	(a) 1.91
			(b) 1.86
			(c) 1.88

there is an unusually large amount of crystallized glass phase present between the silicon nitride grains. This suggests that there may have been incomplete mixing of the liquid phase with the silicon nitride particles during the hot-pressing of this pellet of composition J. Such inhomogeneities may also be removed by a reduction in the total amount of liquid phase in the compact at the hot-pressing temperature.

4.2. Fracture at elevated temperatures

Fig. 3 shows that both compositions B and J exhibit a significant decrease in strength at temperatures above approximately 800° C. The decrease in strength between 800° C and 1375° C is slightly less rapid for composition J while the strength at 1375° C is about 14% of the room temperature strength for composition J and only about 8% of the room temperature value for composition B. This decrease in strength at about 800° C is similar to the behaviour of a relatively impure commercial hot-pressed silicon nitride such as HS 110 grade [6].

The decrease in strength at elevated temperatures that occurs in conventional hot-pressed silicon nitrides is thought to be due to the presence of a magnesium silicate glass phase at the grain boundaries (see Section 1). The low fracture strengths of compositions B and J at elevated temperatures suggest that the strength of the grain boundary bonding in these materials falls rapidly as the temperature increases. At high temperatures this leads to grain boundary sliding under an applied stress giving subcritical crack growth and hence a reduced fracture strength.

The weak grain boundary bonding in these materials at elevated temperatures may possibly be due to the presence of residual glass phases at the grain boundaries. Owing to the complex additives used to prepare compositions B and J, any glass remaining uncrystallized after heat treatment in either of these materials would be a multicomponent glass and so would tend to have a relatively low viscosity at elevated temperatures. This would cause a rapid fall in the strength of these materials as the temperature is increased above the softening point of the glass phase present in each case. This type of behaviour is in agreement with the results obtained (Fig. 3).

The greater reduction in strength for composition B is probably due to the higher calcium content of this material (Table I). Impurities of calcium are known to be deleterious to the high temperature mechanical properties of conventional hot-pressed silicon nitrides [3, 8, 14].

Further evidence for subcritical crack growth in compositions B and J at elevated temperatures is provided by the plots of fracture stress against initial stressing rate (Fig. 4). For polycrystalline ceramics [6, 15] the decrease of fracture strength with decreased stressing rate at high temperatures has been attributed to subcritical crack growth causing the extension of small flaws in the material during loading and a mechanism for this subcritical crack growth has been suggested for hot-pressed silicon nitride [16]. This mechanism involves viscous flow in the grain boundary glass phase at the crack tip. Thus the results obtained here for compositions B and J confirm that there is weak intergrain bonding at elevated temperatures in these materials. The greater sensitivity of the material of composition B to the stressing rate indicates that the rate of subcritical crack growth is sensitive to the relatively high calcium content of this composition. A similar effect has been noted for hot-pressed silicon nitrides containing grain boundary glass phases [8].

The non-linear load–deflection plots obtained for both materials at temperatures above 1000° C, Fig. 5, are similar to those found for conventional hot-pressed silicon nitrides. Such behaviour has been ascribed to a combination of homogeneous plastic flow, due to viscous flow of the grain boundary glass phase, and a change in the compliance of the specimen due to subcritical crack growth [6, 7].

The occurrence of subcritical crack growth before fracture in compositions B and J is also indicated by the appearance of the fracture faces of specimens fractured at 1200 and 1375° C, Fig. 6. The two regions visible on the fracture faces of both materials tested at 1200° C are formed by subcritical crack growth followed by fast fracture. The subcritical crack growth regions are relatively rough and contain large amounts of secondary cracking. This suggests that the subcritical crack growth occurs simultaneously at several crack fronts before the most severe crack initiates catastrophic failure. The fast fracture regions are flat and featureless as there is little stored elastic energy in the specimens at the onset of catastrophic failure. Although there is a different type of crack propagation in these two regions, the detailed microstructure of the fracture faces is very similar

in both regions and for both materials, with fully intergranular fracture in all cases, Fig. 6c.

Although the fracture stress versus stressing rate results indicate small amounts of subcritical crack growth for specimens of both compositions at 1000° C (Fig. 4), no subcritical crack growth regions have been detected on the fracture faces of specimens tested at this temperature. This is due to the small size of these regions and the similarity of the detailed microstructure of the fracture faces for the slow and catastrophic crack growth regions. At 1200° C, the amount of subcritical crack growth before fast fracture, Table IV, increases as the deflection rate decreases, in agreement with the implications of the fracture strength versus stressing rate results.

The fracture faces of specimens of both compositions fractured at 1375° C, Fig. 6d, show only the slow crack growth region. Thus there is very little or no fast crack propagation at this temperature. The large secondary cracks found on the fracture faces of both materials are due to crack growth occurring on several crack fronts simultaneously during failure.

The apparently refractory nature of the inclusions found in both materials confirms that these are particles of crystalline silicate, i.e. enstatite for composition J and forsterite for composition B.

It should be noted that the compositions used in this study are experimental materials which contain higher silica contents, and hence higher total additive contents, than the minimum amount required in each case [9]. There would be some improvement in the properties of these materials if the total amounts of silica and additive were reduced to the minimum quantities possible for each composition. This may reduce any residual glass content and hence possibly the amount of grain boundary sliding at elevated temperatures.

4.3. Young's modulus

The values of Young's modulus at room temperature were found to be similar for compositions B and J at 309 and 324 $GN m^{-2}$ respectively. These results are also similar to measurements of Young's modulus for commercial hot-pressed silicon nitrides, i.e. approximately 300 $GN m^{-2}$ [12]. Thus the presence of small amounts of secondary phases does not seem greatly to affect the modulus of hot-pressed silicon nitride.

The plots of Young's modulus against testing temperature, Fig. 7, show that both materials exhibit similar behaviour, with the modulus remaining constant up to 600° C and then decreasing smoothly between 600 and 1000° C. Composition B shows a greater sensitivity to the testing temperature above 600° C than composition J.

The rapid decrease in Young's modulus that occurs at elevated temperatures for many polycrystalline ceramics has been attributed to grain boundary sliding by a viscous flow mechanism [17]. This suggests that the grain boundaries in compositions B and J are relatively weak above 600° C and allow grain boundary sliding at elevated temperatures. Such behaviour is consistent with the presence of residual glass phases at the grain boundaries in these materials. The higher calcium content of composition B is probably responsible for the greater temperature sensitivity of this material.

5. Conclusions

(1) The room temperature fracture strengths of hot-pressed silicon nitrides containing crystalline magnesium silicate phases are similar to the strength of conventional hot-pressed silicon nitride at a similar stage in its development. Both the compositions studied here fail by fully brittle fracture and the strength-limiting flaws are typically inclusions, which are assumed to consist of the crystalline magnesium silicate phase, or regions of inhomogeneity in the material.

(2) For both materials, the reduction in the fracture stress, the sensitivity of the fracture stress to the initial stressing rate and the non-linear stress–strain behaviour before fracture at elevated temperatures indicate that subcritical crack growth occurs during stressing at temperatures of approximately 1000° C and greater. The rate of subcritical crack growth increases with increasing temperature and with increasing calcium content of the material.

(3) The high temperature properties of these materials are controlled by relatively weak and temperature-sensitive grain boundary bonding. This may be due to the presence of grain boundary glass phases even though there appears to be at least partial crystallization of the glasses present after hot-pressing to give crystalline magnesium silicates.

(4) The presence of small amounts of secondary phases does not greatly affect the value of Young's modulus for a hot-pressed silicon nitride material.

The reduction in Young's modulus that occurs at elevated temperatures for both materials studied here is due to the onset of grain boundary sliding.

Acknowledgements

We are grateful to Dr D. J. Godfrey, Admiralty Materials Laboratory, for his kind assistance in the preparation of the reaction-bonded silicon nitride bend test rams. J. Weston was supported by a Science Research Council Research Studentship from 1973 to 1976.

References

1. P. DREW and M. H. LEWIS, *J. Mater. Sci.* **9** (1974) 261.
2. A. G. EVANS and J. V. SHARP, *ibid.* **6** (1971) 1292.
3. R. KOSSOWSKY, *ibid.* 8 (1973) 1603.
4. K. NUTTALL and D. P. THOMPSON, *ibid.* **9** (1974) 850.
5. W. ASHCROFT, "Special Ceramics", Vol. 6, edited by P. Popper (British Ceramic Research Association, Stoke-on-Trent, 1975), p. 245.
6. F. F. LANGE, *J. Amer. Ceram. Soc.* **57** (1974) 84.
7. S. D. HARTLINE, R. C. BRADT, D. W. RICHERSON and M. L. TORTI, *ibid.* **57** (1974) 190.
8. J. L. ISKOE, F. F. LANGE and E. S. DIAZ, *J. Mater. Sci.* **11** (1976) 908.
9. J. E. WESTON, P. L. PRATT and B. C. H. STEELE, *ibid.* **13** (1978) 2137.
10. F. H. ALDRED, Morgan Refractories Ltd., private communication (1975).
11. A. G. EVANS, *J. Mater. Sci.* **9** (1974) 1145.
12. J. W. EDINGTON, D. J. ROWCLIFFE and J. L. HENSHALL, *Powder Met. Int.* **7** (1975) 82.
13. G. G. DEELEY, J. M. HERBERT and N. C. MOORE, *Powder Met.* **8** (1961) 145.
14. B. D. POWELL and P. DREW, *J. Mater. Sci.* **9** (1974) 1867.
15. S. M. WIEDERHORN, "Fracture Mechanics of Ceramics", Vol. 2, edited by R. C. Bradt, D. P. H. Hasselman and F. F. Lange (Plenum Press, New York, London, 1974) p. 613.
16. A. G. EVANS and S. M. WIEDERHORN, *J. Mater. Sci.* **9** (1974) 270.
17. J. B. WACHTMAN and D. G. LAM, *J. Amer. Ceram. Soc.* **42** (1959) 254.

Received 28 November 1977 and accepted 15 February 1978.